Imaging cyclotron orbits and scattering sites in a high-mobility two-dimensional electron gas

R. Crook, C. G. Smith, M. Y. Simmons, and D. A. Ritchie
Department of Physics, Cavendish Laboratory, Madingley Road, Cambridge, CB3 OHE, United Kingdom
(Received 23 September 1999; revised manuscript received 1 May 2000)

We present experimental images and computer simulations of electron and conduction-band-hole trajectories transmitted between two series constrictions in a two-dimensional electron gas formed at a GaAs/AlGaAs heterojunction. The electric perturbation of a scanning charged probe modified the trajectories to generate the experimental images. In a weak magnetic field, the images revealed cyclotron orbits allowing a measurement of electron and conduction-band-hole energies. Using the same technique, a scattering site caused a 26° change in the trajectories. Computer simulations with localized charge fluctuations in the donor layer, which locally distort the conduction band by 24% of the Fermi energy, reproduced structures seen in the experimental images and features in a related magnetic steering experiment. Conduction-band-holes are holelike quasiparticles in the conduction band with an energy less than the Fermi energy, being equivalent to unoccupied electron states.

Small-angle scattering in low-dimensional systems affects the observation of many quantum phenomena. For example, its strength is a crucial factor in determining the presence or absence of the fractional quantum Hall effect in two-dimensional systems. Small-angle scattering is quantified experimentally from the amplitude of Shubnikov-de Haas oscillations,[1] but this method provides only an average over the entire sample and large scale inhomogeneities prove problematic. In this paper we describe a new imaging technique used to reveal the scattering sites that would be responsible for small-angle scattering in other experiments.

Low-temperature scanning probe microscopy is becoming an invaluable tool for contemporary research of transport phenomena in semiconductor nanostructures. For example: A noninvasive scanning probe that measures charge, generated intricate images of electron compressibility in the quantum Hall regime, revealing meandering filaments and bulbous droplets.[2] A single-electron transistor fabricated on the end of a glass fiber produced surface-potential images of photoionized surface charge, biased surface electrodes, and a cleaved edge.[3] Operating in the quantum Hall regime, a scanning probe used as a local voltmeter, generated profiles and images of the voltage across a Hall bar to investigate edge and bulk currents.[4] A scanning charged probe produced images of electron flux through a single constriction where electrons were backscattered by the probe's electric perturbation.[5,6] A constriction used as a sensitive detector of charge combined with a scanning charged probe, generated images of the probe potential and switching sites, and profiles of the electron density.[7]

Previous work has been limited to a complex noninvasive probe scanning over a subsurface two-dimensional electron gas (2DEG), or a charged probe scanning over a single constriction. We have designed more complex nanostructure devices to operate in conjunction with a scanning charged probe. A new imaging technique reveals spacial information about electron-transport mechanisms in high-mobility heterostructure devices. This technique imaged cyclotron orbits of electrons and conduction-band-holes, and investigated the origin of small-angle scattering, while at lower temperatures quantum coherence effects can be explored. Conduction-band-holes are holelike quasiparticles in the conduction band with an energy less than the Fermi energy, being equivalent to unoccupied electron states. They have been predicted theoretically,[9,10] but have had limited experimental investigation.[8]

An atomic force microscope image of the device at 4.2 K is shown in Fig. 1(a). The visible surface electrodes were fabricated using electron-beam technology as a pair of split gates separated by 4 μm, both with a lithographic gate width of 700 nm. Located 98 nm beneath the surface, a high-mobility 2DEG is formed at a GaAs/AlGaAs heterojunction with a mobility of 300 $m^2\,V^{-1}\,s^{-1}$ and a transport mean-free path of 20 μm. A negative bias applied to the electrodes locally depleted electrons from the underlying 2DEG to define two constrictions in series. Ohmic contacts were made to the 2DEG at the source, the drain, and the central

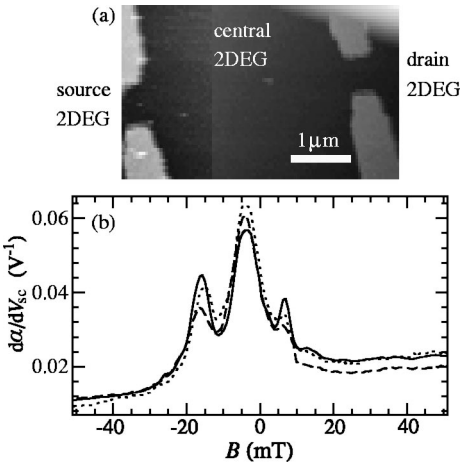

FIG. 1. (a) Atomic force microscope image of the device showing the gate electrodes used to define two series constrictions. (b) Plot of $d\alpha/dV_{sc}$ where $\alpha = I_{center,drain}/I_{source,center}$ is the transfer ratio, against perpendicular magnetic field B with $V_{sc} = -2$ mV, 0 V, and $+2$ mV for the dashed, solid, and dotted lines, respectively. All measurements made at 4.2 K.

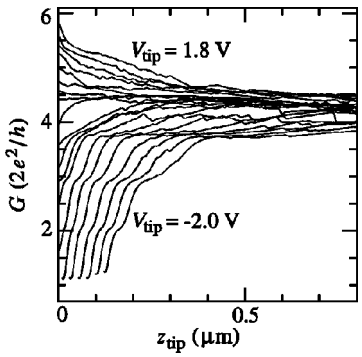

FIG. 2. Plots of constriction conductance G against tip to surface separation z_{tip} for V_{tip} from -2 to 1.8 V.

region. The constriction separating the source from the central 2DEG is referred to as the injection constriction, while the constriction separating the drain is referred to as the collection constriction.

Electrons injected from a constriction into a 2DEG do so as a collimated beam[11] diverging by typically $\pm 15°$ to $\pm 30°$ depending on the electrostatic landscape of the constriction. Collimation can be studied using a collection constriction positioned opposite the injection constriction, such that in a swept perpendicular magnetic field B the angular distribution is steered across the entrance of the collection constriction.[12–14] Such a magnetic steering experiment was undertaken with this device, resulting in the plot shown in Fig. 1(b). The dc source to center bias V_{sc} was -2 mV, 0 V, or $+2$ mV as indicated. An additional low-frequency ac signal of 0.5 mV was applied to the source. The central 2DEG was held at 0 V, and the ac drain current recorded. The transfer ratio $\alpha = I_{center,drain}/I_{source,center}$ is the proportion of injected electrons that are transmitted through the collection constriction. Electrons steered directly through both constrictions created the central peak in Fig. 1(b), which occurs away from $B=0$ T because the constrictions were not perfectly aligned. The energy spectrum of electrons or conduction-band-holes is wider when $V_{sc}=\pm 2$ mV, giving broader structure on the dashed and dotted lines of Fig. 1(b). Troughs observed on both sides of the central peak are later shown to be shadows of single scattering sites, and not quantum-mechanical mode diffraction.[14,15] The plot made at $V_{sc}=+2$ mV demonstrates the existence of conduction-band-holes, corresponding to a beam of reduced electron density through the collection.

The probe is a modified atomic force microscope with a conductive boron-doped silicon tip fabricated on a piezoresistive cantilever.[16,17] To characterize the system, the tip was positioned over a single constriction device. Figure 2 plots constriction conductance G against tip to surface separation z_{tip} at 1.5 K. The different plots have tip biases V_{tip} incremented from -2 to 1.8 V in steps of 0.2 V. The tip was positioned 10 nm above the center of the constriction and slowly retreated to 0.8 μm above the constriction. The constriction conductance clearly detects the changing electric potential as the tip retreats. Several plateaus are seen in conductance that demonstrate the one-dimensional (1D) nature of the constriction. The tip and the sample have different electron affinities, causing a contact potential between the tip and the 2DEG.[3] To counteract the contact potential, a nulling bias is applied to the tip giving a flat response with z_{tip}. From Fig. 2, the nulling bias was measured to be $V_{null}=+0.4$ V.

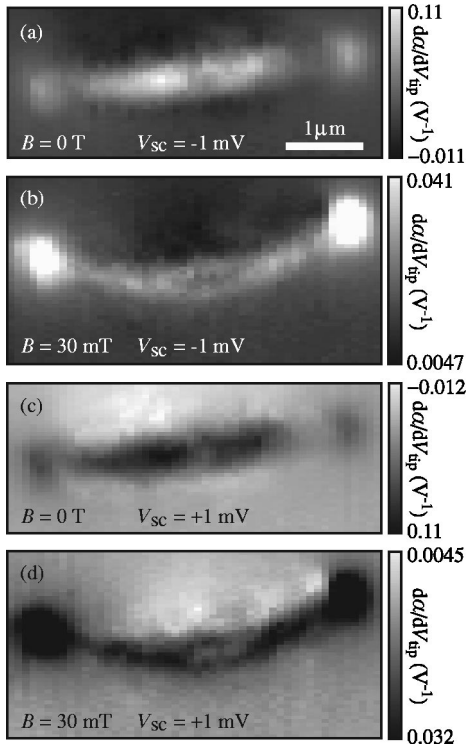

FIG. 3. Experimental images made by scanning the tip 50 nm above the device at 4.2 K, and recording the drain current. In (a) and (c) $B=0$ T, while in (b) and (d) $B=30$ mT. In (a) and (b) $V_{sc}=-1$ mV to inject electrons, while in (c) and (d) $V_{sc}=+1$ mV to inject conduction-band-holes. Note that in (b) and (d) the contrast scale was chosen to reveal detail in the center of the beam, so some points at the ends of the beams are out of range.

Using the double constriction device, the charged probe was scanned over the device surface to investigate electron trajectories in a constant magnetic field. To generate images, a low-frequency ac signal of 0.5 V was applied to the tip. During most of the ac cycle, the signal was less than the nulling bias and the tip perturbation in the 2DEG electrostatic potential repelled electrons and conduction-band-holes. With the central 2DEG held at 0 V, V_{sc} was biased either negative or positive to inject, respectively, either electrons or conduction-band-holes into the central 2DEG. The ac drain current in phase with the tip signal was recorded to determine the image contrast. The tip scanned 50 nm above the device surface to avoid the 30 nm high-surface electrodes.

Figure 3 presents experimental images of the variation of $d\alpha/dV_{tip}$ with tip position at $B=0$ T or 30 mT and $V_{sc}=\pm 1$ mV as indicated. The tip perturbation reduces the electron transfer when it scatters those electrons that would have otherwise been transmitted through both constrictions. Such electrons should be ballistic, as the constrictions are separated by 4 μm and the transport mean-free path is 20 μm. The images therefore reveal all the possible trajectories that travel through both constrictions, which in a magnetic field are the cyclotron orbits. The enhanced transfer seen at both ends of the trajectories is due to the tip electric field directly modifying the constrictions' resistance.[7] The resolution of

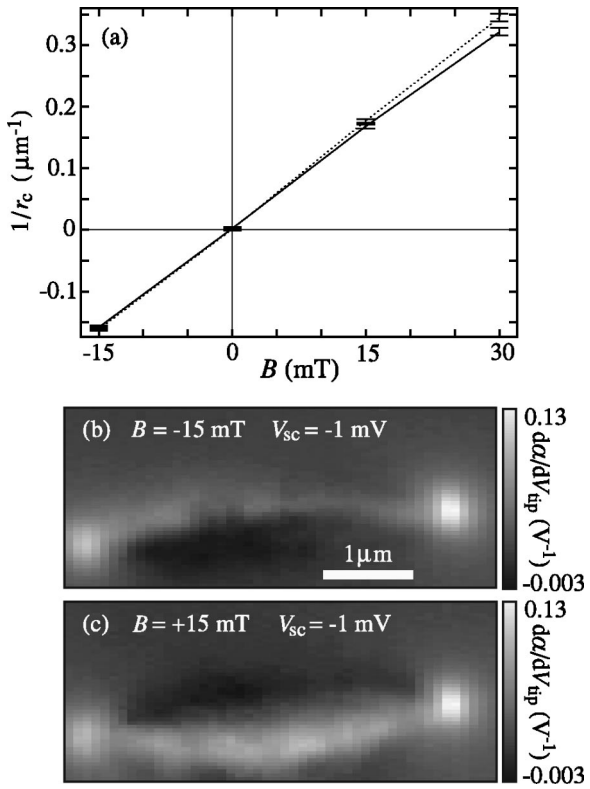

FIG. 4. (a) Plot of $1/r_c$ where r_c is the cyclotron radius, against perpendicular magnetic field B with $V_{sc}=-1$ and $+1$ mV for the solid and dotted lines, respectively. (b) and (c): experimental images with $V_{sc}=-1$ mV and $B=-15$ or $+15$ mT, respectively.

this technique is intrinsically limited by the 2DEG depth,[5] but a lower resolution of approximately 200 nm is observed due to the 100-nm tip radius of curvature combined with the separation between the tip and surface.

A least-squares fit to the peak transfer of each y-direction sweep determines the cyclotron radii of the trajectories in Figs. 3(b) and 3(d). The electrons have more energy than the conduction-band-holes and therefore a larger cyclotron radius. Points at the ends of the trajectories and points where the trajectory appears to split in two were not included in the calculation. The cyclotron radii for electrons and conduction-band-holes are 3.11 ± 0.06 μm, and 2.90 ± 0.05 μm, giving energies of 11.5 ± 0.3 meV and 9.9 ± 0.3 meV, respectively, which fall 0.8 meV to either side of the Fermi energy $E_F=10.7$ meV obtained from Hall measurements. This is consistent with $V_{sc}=\pm1$ mV.

The cyclotron radius r_c is related to B through

$$r_c=\frac{\sqrt{2Em^\star}}{eB}, \tag{1}$$

where E is the electron energy and $m^\star$ is the electron effective mass. Figure 4(a) plots $1/r_c$ against B with data points at $-15,0,+15$, and $+30$ mT. At -30 mT the image contrast was too low to fit a meaningful radius. For points on the solid and dotted lines in Fig. 4(a) $V_{sc}=-1$ or $+1$ mV, respectively. A negative $1/r_c$ denotes the change in the sign of the trajectory curvature observed for negative B. This is shown in Figs. 4(b) and 4(c), which present experimental images at $B=-15$ and $+15$ mT with $V_{sc}=-1$ mV. The gradient of the plots in Fig. 4(a) identifies the different energies of electrons and conduction-band-holes, being proportional to $E^{-0.5}$.

Images, which are not shown here, were also generated at $V_{sc}=\pm1$ and ±2 mV, $B=-36$ to $+36$ mT, $T=1.5$ and 4.2 K, at a gate bias from -1 to -2.25 mV, using several different measurement configurations. All these images exhibited trajectories with the correct cyclotron radii. The images presented were selected to maximize the signal-to-noise ratio without reducing the image resolution. Larger magnetic fields steer the collimated beam away from the collection constriction, which reduces the current and image contrast. With larger V_{sc} the structure becomes less distinct.

We performed computer simulations to investigate the origin of the additional structure seen in the experimental images. In our model, electrons emanated from across the injection constriction with an energy of E_F and a normal angular distribution of standard deviation 17°, which was determined from the envelope of Fig. 1(b). Point charges represented collections or absences of ionized donors,[18] and the resulting potential was calculated including the screening effect of the 2DEG.[19] Note that surface states and deep donor levels known as DX centers[20] will polarize to reduce the donor disorder seen at the 2DEG, so the magnitude of the modeled donor charges is an under estimate. The tip was represented by a point charge of $-54e$, calculated from the capacitance of a conductive sphere above a dielectric boundary, above a conductive plane representing the 2DEG. A method of multiple images through successive approximation[21] for a sphere of radius 100 nm located 50 nm above the dielectric boundary and 98 nm above the conductive plane, gave a capacitance of 0.017 fF. In Fig. 5(a) the simulated trajectories of electrons are shown in the presence two point charges of magnitude $-4.5e$ and $-5e$, both located 60 nm above the 2DEG in the middle of the donor layer and separated laterally by 300 nm, at $B=0$ T. In Fig. 5(b) the simulation was repeated with a count of trajectories passing through the collection constriction plotted against B. The position and charge of the point charges were chosen to reproduce the two distinct side troughs seen in the solid line where $V_{sc}=0$ V in the magnetic steering experiment of Fig. 1(b). The $-5e$ point charge locally distorts the conduction band by $0.24E_F$.

Figure 5(c) shows an image generated by repeating the simulation with the tip at each position on a grid using the same point charge parameters. A count of trajectories passing through the collection constriction determines the contrast of the corresponding pixel. The simulation used $B=0$ T for comparison with Fig. 3(a). To identify features caused by the point charges, the image in Fig. 5(d) was generated in their absence. The enhanced transfer seen bordering the central beam of both the experimental and simulated images occurs when the tip is positioned off the center of the beam, repelling electrons through the collection constriction, and thereby increasing the collector current. There are several features caused by the point charges that are qualitatively similar in the experimental images and the simulation: in the locality of the point charges additional structure is seen, at the collection end of the beam the transfer returns to the background level, and the enhanced transfer bordering the beam is more prominent at the injection end. Figure 5(e)

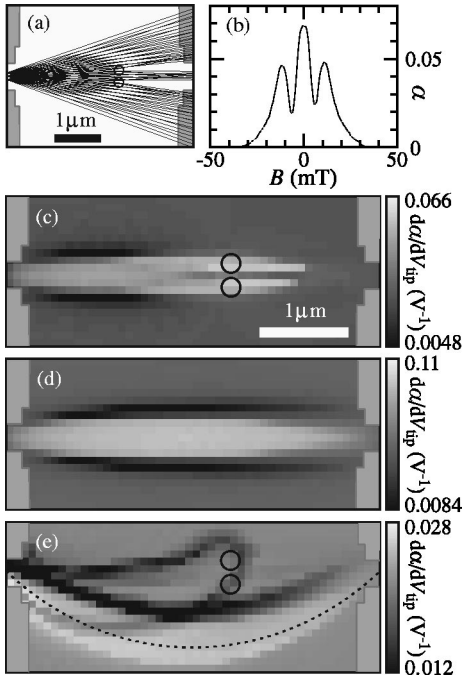

FIG. 5. Computer simulation of electron trajectories. (a) Trajectories emanating from across the injection constriction and repelled away from two point charges positioned at the centers of the circles at $B=0$ T. (b) A count of trajectories passing through the collection constriction plotted against B to simulate the experiment of Fig. 1(b). (c) Image generated by repeating the simulation with the tip at all positions on a grid, including the two point charges positioned at the centers of the circles, at $B=0$ T to simulate the experiment of Fig. 3(a). (d) Image generated without the point charges for comparison. (e) Image generated at 30 mT to simulate the experiment of Fig. 3(b).

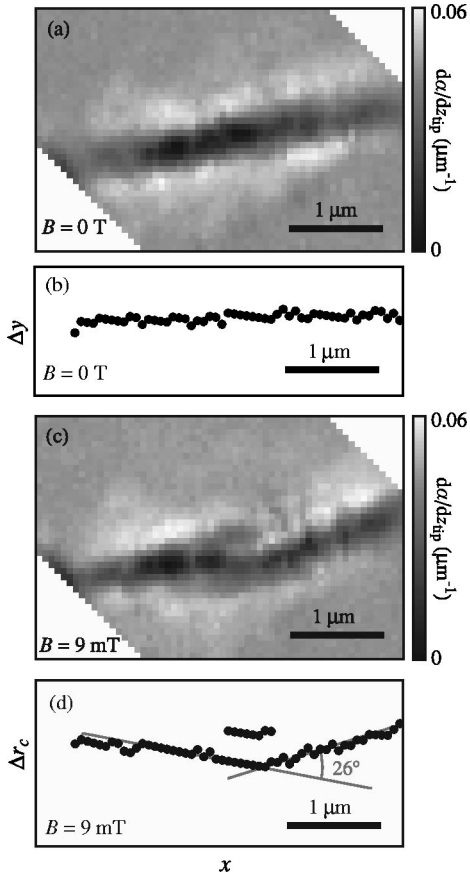

FIG. 6. Experimental images made by scanning the vibrating tip 60 nm above the device at 4.2 K. In (a) and (c) $B=0$ T and 9 mT, respectively, with $V_{sc}=-2$ mV. Contrast minima are plotted in (b) and (d) from images (a) and (c), respectively.

shows a simulation with the two point charges present at $B=30$ mT, E for comparison with the experimental image Fig. 3(c). In both images, the structure seen above the center of the beam is due to the two point charges. Differences between the images arise because the simulation does not include the complete background disorder.

Figures 6(a) and 6(c) show experimental images made using the same device but with a different imaging configuration, at $B=0$ and 9 mT, respectively, and both with $V_{sc}=-2$ mV. The tip was vibrated at 22 Hz with an amplitude of 50 nm and positioned on average 60 nm off the surface, with a dc tip bias of 0 V, which is less than V_{null}. The tip was not scanned in the lower-left and upper-right corners to avoid a collision between the tip and the surface electrodes. With the central 2DEG held at 0 V, the in-phase ac drain current determined the image contrast. The 9 mT image exhibits structure in addition to the increasing curvature with increasing magnetic field. Figures 6(b) and 6(d) show contrast minima of images (a) and (c), respectively, plotted to the same spatial scale with correction for magnetic steering and gate misalignment. Figure 6(d) reveals a distinct 26° change in direction, which is interpreted as the location of a scattering site. We believe the scattering process originates from donor disorder, but not directly from the point charges used in the simulation, as at 9 mT, the trajectories do not correspond to one of the side troughs seen in Fig. 1(b).

A higher spatial resolution is achieved using the vibrating tip configuration due to the sharper functional form of the differential response of the 2DEG electrostatic potential V_{2DEG} with the tip perturbation. If the tip is modeled as a point charge on the device surface, then the tip potential in the 2DEG plane is

$$V_{2DEG} \approx \beta (V_{tip} - V_{null})(r^2 + z^2)^{-\gamma}, \tag{2}$$

where z is the distance from the tip to the 2DEG and r is the radial distance from the tip perturbation in the 2DEG plane. To approximate screening, γ is greater than 0.5, and β is a constant, which is also dependent on screening. When an ac signal is applied to the tip, an ac measurement of V_{2DEG} is equal to

$$V_{tip} \frac{\partial V_{2DEG}}{\partial V_{tip}} \approx V_{tip} \beta (r^2 + z^2)^{-\gamma}. \tag{3}$$

When using the vibrating tip configuration with a dc tip bias, the measurement becomes

$$z \frac{\partial V_{2DEG}}{\partial z} \approx -2\gamma z^2 \beta (r^2 + z^2)^{-(\gamma+1)}. \tag{4}$$

The measurement decreases with r more rapidly for the vibrating tip configuration resulting in a higher resolution.

By studying images from $B=-30$ to $+30$ mT, we sampled a swept area of approximately 2.2 μm^2 for scatter-

ing sites. By comparing images made at slightly different B, the trajectories are sensitive to scattering over a width of approximately 0.25 μm. With the three observed scattering sites, the quantum mean-free path can be approximated as $2.2\ \mu m^2/(3\times 0.25\ \mu m)=2.9\ \mu$m, compared to the transport mean-free path of 20 μm. The ratio of quantum to transport mean-free paths agrees with previous experiments.[22]

In conclusion, we present experimental images and computer simulations of electron and conduction-band-hole trajectories between two series constrictions. A scanning charged probe scattered a collimated beam of electrons or conduction-band-holes to generate the images. This demonstrates that a specifically designed nanostructure device combined with a low-temperature scanning probe can provide new insights into electronic-transport processes. In a weak magnetic field, we imaged cyclotron orbits to measure the energy of electrons and conduction-band-holes. A different measurement configuration produced experimental images that showed an abrupt change in trajectories, which we interpret as the effect of single scattering site. Computer modelling reproduced qualitative features of the experimental images, using absences of ionized donors that locally distort the conduction band by 24% of the Fermi energy. The same donor fluctuations simulated the structure observed in a related magnetic steering experiment. We therefore suggest that donor disorder is the origin of structure in the experimental images and this magnetic steering experiment.

We thank C. H. W. Barnes and C. J. B. Ford for helpful discussions. We acknowledge financial support from the EPSRC and the RW Paul Instrument Fund, and DAR acknowledges Toshiba Research Europe Limited.

[1] P.T. Coleridge, R. Stoner, and R. Fletcher, Phys. Rev. B **39**, 1120 (1989).
[2] S.H. Tessmer, P.I. Glicofridis, R.C. Ashoori, L.S. Levitov, and M.R. Melloch, Nature (London) **392**, 51 (1998).
[3] M.J. Yoo, T.A. Fulton, H.F. Hess, R.L. Willet, L.N. Dunkleberger, R.J. Chichester, L.N. Pfeiffer, and K.W. West, Science **276**, 579 (1997).
[4] K.L. McCormick, M.T. Woodside, M. Huang, M. Wu, P.L. McEuen, C. Duruoz, and J.S. Harris, Jr., Phys. Rev. B **59**, 4654 (1999).
[5] M.A. Eriksson, R.G. Beck, M. Topinka, J.A. Katine, R.M. Westervelt, K.L. Campman, and A.C. Gossard, Appl. Phys. Lett. **69**, 671 (1996).
[6] R. Crook, C.G. Smith, C.H.W. Barnes, M.Y. Simmons, and D.A. Ritchie, J. Phys.: Condens. Matter **12**, 167 (2000).
[7] R. Crook, C. G. Smith, M. Y. Simmons, and D. A. Ritchie, in *Proceedings of the 24th International Conference on The Physics of Semiconductors*, edited by David Gershoni (World Scientific Publishing, Singapore, 1999), p. 190.
[8] J.G. Williamson, H. van Houten, C.W.J. Beenakker, M.E.I. Broekaart, L.I.A. Spendeler, B.J. van Wees, and C.T. Foxon, Phys. Rev. B **41**, 1207 (1990).
[9] G. Bergmann, J. Nodvik, and R. Schäfer, Z. Phys. B: Condens. Matter **101**, 411 (1996).
[10] H. Buhmann, L.W. Molenkamp, R.N. Gurzhi, A.N. Kalinenko, A.I. Kopeliovich, and A.V. Yanovsky, Low Temp. Phys. **24**, 737 (1998).
[11] C.W.J. Beenakker and H. van Houten, Phys. Rev. B **39**, 10 445 (1989).
[12] L.W. Molenkamp, A.A.M. Staring, C.W.J. Beenakker, R. Eppenga, C.E. Timmering, J.G. Williamson, C.J.P.M. Harmans, and C.T. Foxon, Phys. Rev. B **41**, 1274 (1990).
[13] D.R.S. Cumming, H. Ahmed, and T.J. Thornton, Appl. Phys. Lett. **60**, 2755 (1992).
[14] M. Okada, M. Saito, M. Takatsu, P.E. Schmidt, K Kosemura, and N. Yokoyama, Semicond. Sci. Technol. **7**, B223 (1992).
[15] T. Ando, Phys. Rev. B **44**, 8017 (1991).
[16] M. Tortonese, R.C. Barret, and C.F. Quate, Appl. Phys. Lett. **62**, 834 (1993).
[17] Park Scientific Instruments, Sunnyvale, California 94089.
[18] J.A. Nixon and J.H. Davies, Phys. Rev. B **41**, 7929 (1990).
[19] T. Ando, A.B. Fowler, and F. Stern, Rev. Mod. Phys. **54**, 437 (1982).
[20] M. Hauke, J. Jakumeit, B Krafft, G. Nimtz, A. Förster, and H. Lüth, J. Appl. Phys. **84**, 2034 (1998).
[21] P. Lorrain and D. Corson, *Electromagnetic Fields and Waves*, 2nd ed. (Freeman, San Francisco, 1970), p. 150.
[22] P.T. Coleridge, Phys. Rev. B **44**, 3793 (1991).